Chapter 10
Aircraft Engine Fan Blade Design: Impact Tolerance Prediction of Partially Filled 3D Printed Aluminum, Titanium, and PEEK-Filled Waste Metal Dusts

Shade Rouxzeta Van Der Merwe, Daniel Ogochukwu Okanigbe, Dawood Ahmed Desai, and Glen Campbell Snedden

10.1 Introduction

The gross domestic product (GDP) contribution of the air transport sector in South Africa (SA), comprising airlines and its supply chain, is estimated at US $5.2 billion (GDP). An additional US $4.3 billion, or US $9.4 billion, of the nation's GDP is supported by international visitor spending [1]. In order to maintain competitiveness in the global tourism industry, further technological developments in aircraft operation are motivated by this support, which helps to increase SA's GDP growth. And as a result of this need for further technological development in operational aircraft, opportunities are formed for the discovery of new materials, unique design concepts, and the production of engineering components [2, 3].

Cheap structural ceramics, such as the Mullite Rich Tailings (MRT) from density separation of copper smelter dust [4, 5], will undoubtedly find a position to play a significant part in the consequent technological developments in the aerospace industry [6] by taking use of these prospects. The use of ceramic matrix composites in the hot section of engines has recently gained increased support from aircraft

S. R. Van Der Merwe · D. A. Desai
Department of Mechanical and Mechatronics Engineering, Faculty of Engineering and the Built environment, Tshwane University of Technology, Pretoria, South Africa
e-mail: vandermerweR1@tut.ac.za

D. O. Okanigbe (✉)
Department of Chemical, Metallurgical and Materials Engineering, Faculty of Engineering, Tshwane University of Technology, Pretoria, South Africa

Pantheon Virtual Engineering Solutions, Nigel, South Africa
e-mail: okanigbedo@tut.ac.za; okanigbeogochukwu@gmail.com

G. C. Snedden
Department of Mechanical Engineering, Aerospace Systems Research Group Gate, University of KwaZulu-Natal, Durban, South Africa

D. O. Okanigbe, A. P. Popoola (eds.), *Resource Recovery and Recycling from Waste Metal Dust*, https://doi.org/10.1007/978-3-031-22492-8_10

engine manufacturers, in line with this school of thought [7, 8]. Mullite ceramics are capable of operating at temperatures of up to 1600 °C and have a high thermal shock, claim Zhao et al. [9], Lee, Zhu and Lima [10], and Suleimanov et al. [11]. These characteristics make this structural material more appealing for aerospace applications than standard materials; in particular, because it reduces weight, needs less cooling air, and as a result helps to lower fuel consumption and increase aircraft performance [10, 12].

However, Padture [13] asserts that it is doubtful to fully utilize the capabilities of MRT to simply replace metallic or polymer components in existing propulsion systems, such as the aircraft engine fan blade (Fig. 10.1), with mullite ceramics (e.g., MRT). The processing and production of components using these novel composites [14] will also continue to be difficult [15], but they offer a fertile ground for innovation, thus they must be included in the endeavor [16]. For example, using impact tolerance of partially filled 3D printed turbine component as a function of varied infill densities, will need to be developed in order to account for the excessive cost of extensive component-level testing under realistic engine conditions [17–19]. Additionally, reliable physics [20–22] and mechanisms-based models [23] that describe the behavior of the constituent MRT [13, 24, 25], the composites [26–28], and the component at temporal scales [29].

In order to coordinate the operations of the composites, i.e., of reinforcement (MRT) and matrix (metal or polymer), while embracing and utilizing the growing complexity at temporal scales, it will be necessary to design aircraft components with distributed systems. Noting that achieving necessary qualities inside composites that cannot be satisfied by existing materials will be necessary for the expedited development of new MRT reinforcing.

Fig. 10.1 Picture of the Boeing 747's engine with its fan blades. (Source: Google image)

The process must be put through an integrated design-modeling-experiment-manufacturing strategy, which should span composites-3D printed components-system hierarchy, in order to test these desired qualities. A strategy that, for accelerated development, should embrace integrated computational materials engineering and the materials genome initiative principles. By doing this, the MRT's full potential can be realized.

Furthermore, a thorough understanding of material cost savings associated with 3Dprinting aircraft components is necessary to fully realize MRT's potential for creating composites for aerospace applications. During the manufacturing of aircraft components using composite materials, materials' cost savings can be realized by optimizing 3D process parameters (especially infill density) to get the best percentage material content [30–32].

There is no need to fill the interior of 3D printed components, according to Moradi, Meiabadi, and Kaplan [33], because the optimized specimen has better mechanical properties, a lighter part weight, a faster build time, and lower production costs than the filled specimen. Consequently, fuel consumption was decreased as a result of the lighter components made under these circumstances.

It is crucial to research the possibilities of using MRT as reinforcement in the development of aerospace materials for the production of 3D printed engineering components. More specifically, how this waste can further improve material cost savings and produce higher mechanical qualities like impact tolerance. This idea is supported by the proposed study, which tries to optimize the infill density of 3D printed turbine blades and choose the best construction capable of withstanding the highest expected loads with the least amount of material and production time.

10.2 The Problem Statement

The degree to which specific process parameters like time and material are managed can determine whether the impact tolerance of 3D printed components is acceptable or unwanted. The best conditions, approach, and/or requirements have not yet been discovered to produce the best impact tolerance of partially filled 3D printed components from a combination of all the characteristics. The goal of maximizing profit in the aerospace industry is defeated since, in order to obtain optimum tensile strength of a 3Dprinted turbopump component, an infill is frequently 100% filled. This implies greater expenses (i.e., in terms of time and material) and heavier components.

Sub-problem 1 What are the main factors affecting the 3D printing process?

This will specify the components of the 3D printing procedure necessary to generate results of material advantages to be assessed for optimization. When changed, these components, also known as influential parameters, have a significant impact on the output and define the functionality and output of the 3D print process.

Sub-problem 2 What are the optimization objectives?

This forces the researcher to establish design goals in the form of objectives, the anticipated outcomes of the 3D printing process, and which elements of these outputs should be maximized and which elements should be minimized. In order to achieve the overall goal of increasing the impact tolerance of partially filled 3D print components, this will help determine what outcomes need to be traded off in exchange for gains on other sides, what properties should increase and what properties must decrease, what beneficial aspects need to be strengthened and what harmful aspects need to be weakened.

Sub-problem 3 What strategy will be used to model the problem and improve the model simulation's outcomes?

Sub-problem 4 Which set of ideal parameters best addresses the research problem's numerous objectives?

This study's optimization deliverable is a multiobjective problem with multiple potential solutions rather than a single ideal one. In order to achieve the optimal combination or sets of combinations, we must now solve the problem of defining the amount of weights and impact coefficients to be assigned to the various sub-objectives, designating them in order of importance while limiting those with unclear possibilities.

10.3 Research Hypotheses

For this study, the following tentative assumptions have been implemented to serve as the foundation for addressing the key questions which this research presents.

Hypothesis 1 The following elements comprise the parameters for this optimization problem that affect the anticipated result of the 3D print:

(a) 3D print attributes

- Speed
- Size
- Accuracy
- Durability
- Material

(b) Factors defining material behavior

- Temperature
- Pressure
- Strain rate
- Material content (% infill)

(c) Mechanical component tolerance

- Size
- Shape
- Volume

Hypothesis 2 The results of an impact tolerance test on a partially filled 3D component are induced tensional residual stresses, material hardening, and uniaxial yield stress as a result of brittle deformation, therefore optimization goals must be specified for all three results. These consist of:

- Tensional residual stress maximization
- Reduced material hardening
- Reduced uniaxial yield stress as a result of brittle deformation

Hypothesis 3 Impact tolerance of a 3D print can be modeled as short, intense pressure pulses from an outside item that collide and transmit energy to the material. The primary factors governing the transfer of energy can be quantitatively modeled and evaluated using finite element material modeling. In addition to ABAQUS, the parametric optimization software tool Isight can find the best combinations that will cause the 3D printing process to deliver the desired response(s).

Hypothesis 4 It is anticipated that the optimization process will produce more than one feasible solution. In this scenario, the designated sub-objectives can be iterated with respect to the various responses they produce, with weights and scaling factors arranged in order of importance and impact. Using a decision-making matrix, a set or sets of multiple combinations of the best solutions can then be obtained.

10.4 Research Objectives

10.4.1 Main Objectives

The main objectives of the proposed research study are to predict the impact tolerance of a 3D printed turbine component that is partially filled and to identify the subsequent best infill.

10.4.2 Sub-Objectives

The primary goal of this study will be accomplished by simulation and experimental model validation. The following set of supporting goals will help to attain this main goal:

1. The creation of a numerical turbine model using finite element analysis (FEA).
2. Examine the impact tolerance of the turbine developed at various infill levels (i.e., 20%, 25%, 30%, 35%, 40%, 45%, 50%, 55%, 60%, 70%, 75%, 80%, 85%), as well as the impact on the deformation pattern (Plastic or brittle).
3. To experimentally check the consistency of the FEA model as well as to validate it analytically using the moment of inertia methodology.
4. Last but not least, suggest the ideal infill for a 3D printed turbine component that will conserve both time and material.

10.5 The Assumptions

To optimize the infill density of the 3D printed turbine blade and choose the best structure able to handle the highest expected loads with the least amount of material and manufacturing time, finite element analysis will be used. The study and resolution of the issue will be conducted under the following set of presumptions in order to do this:

1. The foreign object strikes the turbine blade at an angle that is normal to its surface.
2. The entire procedure conserves energy.
3. Each disk's blades are permanently fastened to the disk and have the same characteristics.
4. Radial displacement and torsion are disregarded because it is presumed that the blade angle motion is minimal.
5. The ith fan blade's motion consists of out-of-plane motion in the axial direction of the rotor and in-plane motion along the circumferential direction of the disk.
6. Homogeneous and isotropic mechanical characteristics of unmixed material, metal matrix composites, and polymer matrix composites will be assumed.
7. Unmixed materials, metal matrix composites, and polymer matrix composites are assumed to act linearly ideal elastically, which means that the law of linear elasticity is applied to each individual layer.
8. The apparent-level compressive modulus (E_c) measured experimentally and combinations of infill densities will be used to represent the unmixed material, metal matrix composites, and polymer matrix composites as a continuum (20%, 25%, 30%, 35%, 40%, 45%, 50%, 55%, 60%, 65%, 70%, 75%, 80%, 85%).
9. The hypothesis excludes flaws like fractures and air bubbles.
10. It is assumed that the layers formed by the particle and matrix composition are orthotropic and properly adhered to one another.
11. Because the particles are not evaluated separately from the matrix or the binder layer, interface effects are disregarded.
12. The various layers are perfectly connected to one another. When loads are applied, it is presumed that relative slip won't happen.

10.6 The Project Deliverables

When this research study is finished, it should produce the following results:

1. A flexible, finite element-based model that has been experimentally verified can be used to forecast the impact tolerance of a partially filled 3D printed turbine component.
2. A process that can be used to increase the impact tolerance of a 3D printed, partially filled turbine component.
3. Identification of the optimal process parameter combinations that influence the outcomes of 3D printing methods.

10.7 Importance of Study

This study's importance rests on:

10.7.1 Benefits to the Academia, Research, and Development

1. In order to maximize benefits and reduce manifestation of side effects of the surface treatment process, the research aims to examine and provide answers regarding how, where, when, and which ways laser peening should be employed in the surface treatment of LP steam turbine blades.
2. It offers methods for methodically and nondestructively enhancing the mechanical characteristics of turbomachinery components in an effort to increase reliability, cut downtime, lower the likelihood of in-service failure, and extend the useful life of steam turbine blades.
3. The results of this study will be helpful for improving material tensional residual stress in a variety of production and manufacturing applications, including the power, energy, production, oil and gas, aviation, and automotive industries, where turbopump machinery is a crucial component of operations and production.
4. Finally, the research's uniqueness may lead to a patent, which would add to the body of knowledge by encouraging other studies into asset integrity management and additive manufacturing. When this research is finished, journal articles in reputable, high impact journals and presentations at national and/or worldwide peer review conferences are also promised results.

10.7.2 Benefits to the Industry

The results of this research will provide the industry with the following advantages in addition to the other two listed above:

1. The creation of best practice recommendations for 3D printing parts in industry to remain compatible with the systems of the fourth industrial revolution.
2. Designs can be strengthened where they are weak without necessarily adding weight or substance.
3. Decrease in equipment downtime, inspection time, and maintenance expenses as a result of replacing faulty components while they were still operating.
4. A significant decrease in the amount of time needed to complete 3D printing tasks on plant and equipment parts during maintenance sessions. Prolonging the equipment's overall usable life.
5. Enhanced industrial and power plant operation and maintenance efficiency.
6. Increased guarantee of the components used in industry's safety and quality.

10.7.3 Benefits to South Africa

The national development goals of energy security and innovation to commercialization are perfectly aligned with this research. Therefore, the research output will contribute to a greater South African society in addition to benefiting academics and business, and it will be highly appealing to the goals of the government of the republic of South Africa in the following areas:

1. Decrease in the price of producing electricity
2. Improved industrial and power plant operation and maintenance efficiency
3. Reduction in the likelihood that components of operating industrial or power plants would collapse catastrophically
4. Increased assurance of the components' quality used in industry

Creation of test models and protocols to certify and accredit replacement component suppliers for industrial application.

10.8 Overview of the Study

Chapter 1 Acts as the study's introduction. It gives the study background, the problem statement, the hypotheses, the research technique, the assumptions, the delimitations, the project planning, and the research project's financial budget. Additionally, the dissertation's whole chapter-by-chapter research project outline is provided.

Chapter 2 Consists of a study of the literature done on blade containment difficulties.

This covers relevant literature found in the standards as well as earlier studies, books, conference reports, and more. This chapter will also include further studies on the actual experimental setup, tools, and equipment.

Chapter 3 Introduces mathematical modeling of phenomena pertinent to the study's goals.

Chapters 4 and 5 Focus on developing material models and a numerical model to predict impact tolerance using ABAQUS FEA software.

Chapters 6 and 7 ABAQUS's complementary parametric optimization software tool Isight will be used to optimize the impact tolerance simulation's key parameters in order to find the best combinations that will lead to the impact tolerance process's desired response or responses.

Chapter 8 Includes a description of the experimental characterization, which will cover the actual setup, analysis, and results tabulation. The experiments will be carried out when the physical testing specimen has been prepared.

Chapter 9 Presents the research's overall findings and results, along with any comparisons and explanations of the findings.

Chapter 10 Broad conclusions about the work, acknowledges unresolved issues, and makes suggestions for future work that can be done. This chapter will also include advice on how to deal with the underlying issue.

Chapter Summary
The reader is introduced to the research study in this chapter, which also emphasizes the key reasons why it should be pursued. This part of the research project also includes the problem statement, project objectives, research methodology, and study scope. The background and literature review of this study effort are presented in the following chapter. It comprises the theoretical information required to comprehend this research endeavor and its relevance by making use of prior research.

10.9 Literature Review

10.9.1 Introduction

Short lead times for product development without sacrificing the quality of the developed part are required by modern production processes. Rapid prototyping (RP) is one of the unique manufacturing techniques and materials that have been developed as a result of this [34–38]. Additive manufacturing, often known as 3D

printing, refers to procedures that manufacture objects by depositing material layer by layer without the need for finishing, as with traditional manufacturing processes.

Using only the fabrication machine, additive manufacturing enables the direct production of intricately structured items from their computer-aided design (CAD) models. Low maintenance costs, easy material swapping, a cool working environment, supervision-free operation, and small size are some of this technique's primary benefits [39]. The typical method for product development among manufacturers is now 3D printing [40, 41]. Production in a computer-integrated industrial environment is facilitated by 3D printing.

Manufacturing processes can be significantly improved by integrating 3D printing and concurrent engineering [42]. Fused Deposition Modeling, or 3D printing, is the most popular method (FDM). This method involves layer-by-layer application of melted filament, often made of Acrylonitrile Butadiene Styrene (ABS) or polylactic acid (PLA), which finally cools to create the solid object. The plastic filament is melted by an extruder that may move in the x-y plane and is then deposited on a bed that moves in the z direction to create the final 3D item.

FDM models reduce waste and make the process environmentally benign because they can be recycled [43]. The unique feature of the FDM method is its capacity to locally regulate the mechanical, density, and porosity characteristics of the created object [44]. FDM is a technique that can be used to create functioning items in addition to prototypes. The FDM needs to be improved in several ways in order to be used as a manufacturing tool. These include improved surface polish, tighter tolerances, and better dimensional control. Additionally, a wider variety of polymers should be available for usage, and prototyped parts' mechanical qualities should be improved to preserve their integrity while in use [45].

Contrary to the majority of manufacturing processes, the values of process parameters in additive manufacturing techniques can often be more important than the characteristics of the part material. Different sets of process settings will result in completely different attributes for parts with the same shape, such as strength [46, 47] or precision [48]. Each set of process variables, including bed temperature, layer thickness, infill pattern, and infill density, will result in a unique component structure, which will in turn provide unique mechanical property values.

Consequently, the papers under the following subheadings will be evaluated in this review section:

1. A review of publications on the impact of raster orientation and air gap on mechanical properties of 3D printed components.
2. A review of articles on how the mechanical qualities of 3D printed components are affected by printing speed, binder characteristics, infill rate, and layer thickness.
3. An analysis of papers examining the impact of PEEK use against ABS on the mechanical characteristics of 3D printed components.
4. An analysis of research on the impact of the infill pattern and density on the mechanical characteristics of 3D printed components.

10.9.2 Review of Publications: Present and Past

10.9.2.1 Review of Articles on the Impact of Infill Density on the Mechanical Characteristics of 3D Printed Components

Using the Taguchi approach, Abbas et al. [49] assessed the tensile, compressive, and bending strength of polylactic acid (PLA) samples by adjusting the infill density and other process variables. With increasing infill density, a rise in strength was seen. While cutting back on the infill density, printing time was significantly reduced.

The same scenario played out as an increase in infill density led to an increase in tensile strength in a related study by Srinivasan et al. [50]. According to the authors, an infill density that yielded a tensile strength of 17.38 MPa at 100% infill produced a tensile strength of 32.12 MPa.

By adjusting the infill density and pattern, Ebel and Sinnemann [51] created PLA and ABS samples. It was determined that PLA samples had greater tensile strength than ABS samples. Additionally, samples that were fully filled were stronger than those that were partially filled.

This line of reasoning was documented in the study by Tanveer, Haleem, and Suhaib [52], not only for the impact strength but also for the tensile strength of 3D printed PLA parts. In their research, all of the FDM process parameters were held constant while the infill density was changed (A = 100%, B = 75%, C = 50%). According to the combinations listed in Table 10.1, a total of nine kinds of specimens were claimed to have been created. Following are the results of this study's findings:

1. That substantially less raw material can be used by stacking layers with various infill densities.
2. That by keeping the infill density of inner layers dense and the infill density of outer layers less dense, the tensile strength of the 3D printed PLA part can be improved. These arrangements, according to the authors, give resistance to crack development while fostering flexibility in the interior structure.

Table 10.1 The way the infill density is organized

S/N	Classification (C)	Infill density		
		Outer layer	Inner layer	Outer layer
1	A	100	100	100
2	B	75	75	75
3	C	50	50	50
4	ABA	100	75	100
5	BAB	75	100	75
6	ACA	100	50	100
7	CAC	50	100	50
8	BCB	75	50	75
9	CBC	50	75	50

Table 10.2 The specimen's weight and impact resistance

C	Izod strength (KJ/m^2)	Weight (g)	Charpy strength (KJ/m^2)	Weight (g)
A	4.2	24.23	4.75	12.12
B	2.9	20.02	3.45	9.87
C	2.42	17.42	2.75	8.80
ABA	1.7	19.14	3.00	10.84
BAB	1.85	18.57	3.75	10.12
ACA	2.58	19.82	2.90	9.88
CAC	3.15	17.50	3.50	9.11
BCB	2.75	22.70	1.90	9.84
CBC	3.54	21.35	2.10	9.27

3. For the impact test, the infill density and impact strength have a linear relationship, as shown in Table 10.2. Impact strength was found to decrease when different infill densities were mixed.
4. Unlike in the case of tensile strength, impact strength rises when the inner layer has a higher infill density and a lower density outer shell.

The observations made by Abbas et al. [49], Srinivasan et al. [50], and Ebel and Sinnemann [51] were also made in a different study by Gunasekaran et al. [53]. According to the authors, the mechanical characteristics of PLA printed specimens improved as infill density rose from 25% to 100%. The hardness, tensile strength, impact strength, and flexural strength values for the PLA specimen printed with a 100% infill density were 97 HRC, 53 MPa, 70 J/m^2, and 53 MPa, respectively. The authors suggested using PLA specimens produced with a 100% infill density to create components for a variety of applications in light of their findings.

But according to the research by Moradi, Meiabadi, and Kaplan [33], there is no need to fill the interior of 3D printed parts because the optimized specimen has better mechanical properties, a lighter part weight, requires less time to build, and costs less to produce overall than the filled specimen.

10.9.2.2 A Review of Publications on Selective Laser Melted Aluminum Alloys for Development of Aerospace Components

Aluminum is frequently combined with Zn, Cu, Mg, Mn, and Si to create age-hardening alloys, casting alloys, and work-hardening alloys, as indicated in Fig. 10.2 [54–57] according to AtiK et al. [54]. In this review, the emphasis is on the mechanical properties of aluminum-silicon (Al-Si) alloys produced using the metal additive manufacturing technology of selective laser melting (SLM).

Due to their castability and weldability, Al-Si alloys are frequently suited for SLM processing. According to findings in the literature [59–63], AlSi10Mg and AlSi12 are the most often used SLM aluminum alloys. These publications describe

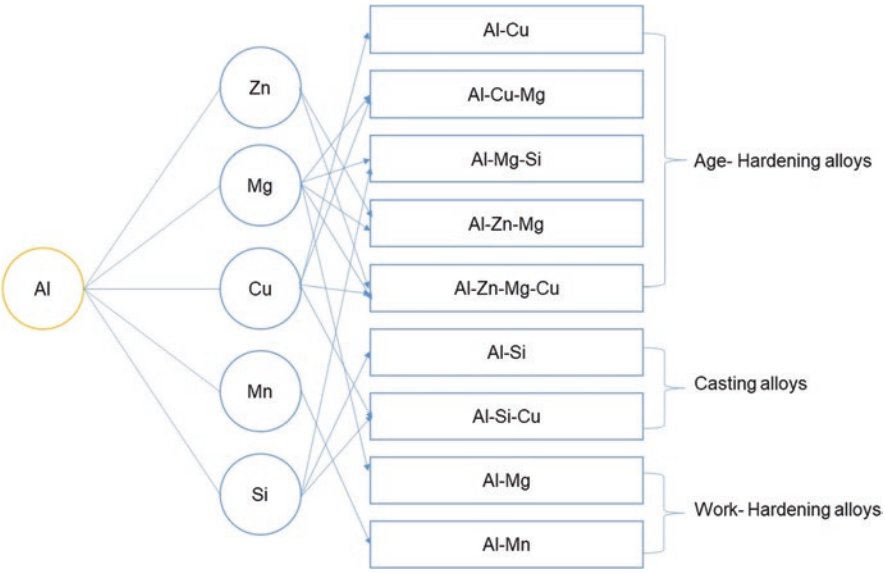

Fig. 10.2 Important aluminum alloys. (Adapted from Altenpohl [58])

the four basic types of Al-Si aluminum alloys and the classification of SLM-processed aluminum alloys in terms of process optimization.

These publications provided an orderly criticism of several types of investigations into the mechanical characteristics of SLM aluminum parts. It is noted that the majority of these papers have focused on the tensile mechanical characteristics of SLM aluminum alloys. A relative few research have been done on the dynamic behavior of 3D printed components in tension and compression [59–61, 64, 65], fatigue [66, 67], impact tolerance [62, 68], wear [69, 70], and flexural response [63, 71].

10.9.2.3 An Analysis of Articles on the Use of Selective Laser Melting to Create PEEK for Aerospace Components

Polyetheretherketone (PEEK) is increasingly being employed in selective laser sintering (SLS), as indicated by Patel et al. [72], due to its good mechanical and thermal properties as well as biocompatibility. It is known that SLS powder's qualities control how well components can be processed and produced. However, there is still more research needed to understand how this thermal history affects part quality. As a result, Patel et al. [72] used spectroscopic, morphological, and rheological characterizations to assess changes in thermally treated PEEK powder. Although the particle size and form of the melted PEEK powder were significantly raised in viscosity, with somewhat improved flowability, the authors observed that crystallinity rose only slightly within the first 2 h.

Wang et al. [73] reaffirmed that PEEK is an engineering thermoplastic with outstanding biocompatibility and strong mechanical qualities, confirming the claim stated by Patel et al. [72]. They agree that PEEK's high viscosity and high melting temperature pose difficulties for FDM. For the best surface quality and enhanced mechanical qualities, authors employed finite element analysis (FEA) to simulate the melting conditions and fluidity of PEEK in a flow channel. For consistency in the outcomes for the mechanical characteristics, microstructure, and surface quality of printed PEEK parts, models were experimentally validated. Based on the results, the authors concluded that layer thickness of 0.1 mm, printing at a speed of 20 mm/s, and a higher heating temperature of 440 °C [74] can increase the density of PEEK parts while reducing internal defects, binding layers, and infill filaments, and surface roughness to the absolute minimum.

SLS is one of the cutting-edge additive manufacturing techniques that can construct the geometrically complicated structure from a three-dimensional CAD model, according to Wang et al. [75]. PEEK is one of the materials that can be used for SLS and has drawn considerable interest because of its great characteristics [72]. Thermally induced phase separation (TIPS), a new methodology was used by the authors to manufacture pristine PEEK and PEEK/CNT composite powders with nearly spherical shapes, desirable particle sizes, and size distributions for SLS applications. It was discovered that the powders created with TIPS had good flowability and processability. According to the results, PEEK's storage and loss modulus were both increased with the addition of 0.1% CNT.

10.9.2.4 A Review of Works on Selective Laser Melting of Ti–6Al–4V for Use in Aerospace Parts

The authors of Knowles, Becker, and Tait's studies [76] stated that SLM of Ti–6Al–4V has enormous promise in the aerospace and biotechnology sectors. The utilization of a concentrated laser beam using SLM to melt successive layers of metallic powder into intricate components was also disclosed by the authors. The authors claim that this method has the potential to generate significant residual strains caused by heat. They believe that at relatively modest cyclic stresses, these residual stresses, along with microflaws/pores from the underlying fabrication process, have the potential to produce premature fatigue fracture initiation and propagation. In order to ascertain residual stresses within SLM Ti–6Al–4V specimens and comprehend the underlying mechanisms for SLM Ti–6Al–4V's effective industrial application, the hole-drilling strain gauge method was used.

Beta Ti-alloys are most suited for applications requiring high fracture toughness and ductility, such as the aerospace and biomedical industries, as indicated by Madikizela, et al. [77]. The authors also said that the aerospace sector has looked into SLM of the alpha + beta Ti–6Al–4V alloy in great detail. Despite the success in fabricating small parts, it is difficult to build big parts with an acicular microstructure. Ti–6Al–4V has an acicular microstructure, which reduces its ductility and fracture toughness (10% elongation), causing components to distort and delaminate

from the base plate even before they are finished because of stress buildup. This led the authors to investigate the microstructure and mechanical characteristics of two-phase Ti–6Al–4V and beta titanium alloy Ti-38,644 in their as-built state. The findings demonstrated that Ti-38,644 had a complete microstructure and lower strength than Ti–6Al–4V, which had a fine martensitic structure inside columnar grains. Ti-38,644 had three times the percentage elongation of Ti–6Al–4V, indicating the possibility of fabricating massive parts from it.

Yang et al. [78] studied the SLM-produced Ti–6Al–4V crystallographic pattern at various laser energy densities. The outcomes demonstrated that the mechanical anisotropy of SLMed Ti–6Al–4V samples is significantly influenced by the crystallographic orientation dependent on laser energy density (LED). The SLMed Ti–6Al–4V samples have a completely martensite microstructure. With laser LED, the content of prismatic orientations rises from 101 to 269 J/mm^3, while the proportion of basal orientations falls in martensites. The tensile properties of samples that were created horizontally and vertically differ, according to the authors, and this anisotropy is visible with LED. Higher Schmid factor values of grains in vertically built tensile samples than in horizontally built tensile samples are thought to be the cause of anisotropy.

Conclusion on Literature Review

In order to identify the knowledge gap and research priorities from the perspective of aerospace applications, these review section analyzed various types of investigations on the mechanical properties of SLM aluminum, PEEK, and Ti–6Al–4V parts.

Conclusion: Although 3D printed airplane parts are frequently strong and lightweight, there is still a significant knowledge gap when parameters like infill density are set to 100% for maximum tensile strength of printed components. This knowledge gap is evident from the literature review.

Thus, the prediction of impact tolerance for a partially filled 3D printed turbine component became the study's main focus.

10.10 Research Methodology

In order to address the highlighted problems, numerical and experimental methods will be employed.

10.10.1 Material Study and Selection

10.10.1.1 Material Study

Aluminum alloys, titanium alloys, thermoplastics, high-strength steels, nickel metal alloys, magnesium alloy, and composites are the most often utilized structural materials in commercial aerospace, and together they make up more than 90% of the weight of airframes.

10.10.1.2 Material Selection

Unmixed Material

Out of the aforementioned materials, three were identified and chosen for this investigation. Table 10.3 lists these three materials along with their mechanical material characteristics.

Composite Materials

As particulate reinforcements to the pure materials (i.e., Aluminum 6082-T651 alloy, PEEK 1000, Ti–6Al–4V alloy), waste copper dust (WCD) and mullite-rich tailings (MRT) from density-separated WCD will be used.

These combinations of matrix and reinforcements will result in the following categories of composites (aluminum composites, PEEK composites, Ti–6Al–4V composites), which are depicted in Figs. 10.3, 10.4, and 10.5, respectively:

Table 10.3 The mechanical material properties (MMP) of the aluminum 6082-T651 alloy, PEEK 1000

MMP	Units	Materials		
		Aluminum 6082-T651 alloy	PEEK 1000	Ti–6Al–4V alloy
Elastic modulus (E)	GPa	70 [79, 80]	3.6 [79]	107 [77]
Density (ρ)	kg/m^3	2700 [79, 80]	1304 [79]	2560 [81]
Poisson's ratio (ν)		0.33 [79, 80]	0.4 [79]	0.33 [82]
Coefficient of Kinetic friction (μ)		1.4 [79, 80]	1.0 [79]	0.25 [83]

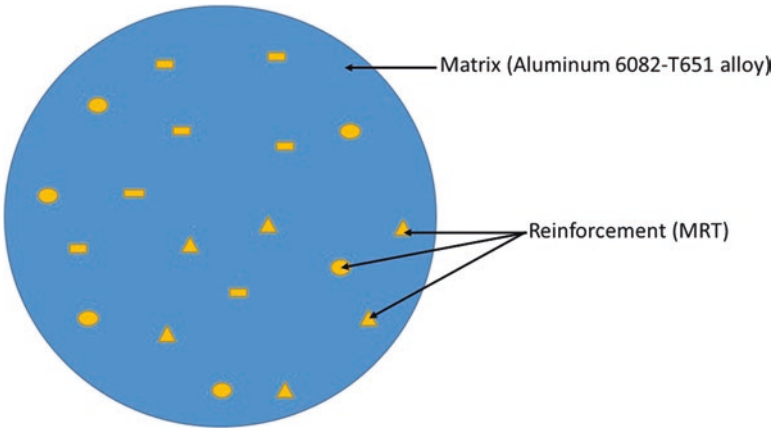

Fig. 10.3 Image of Aluminum 6082-T651-composites

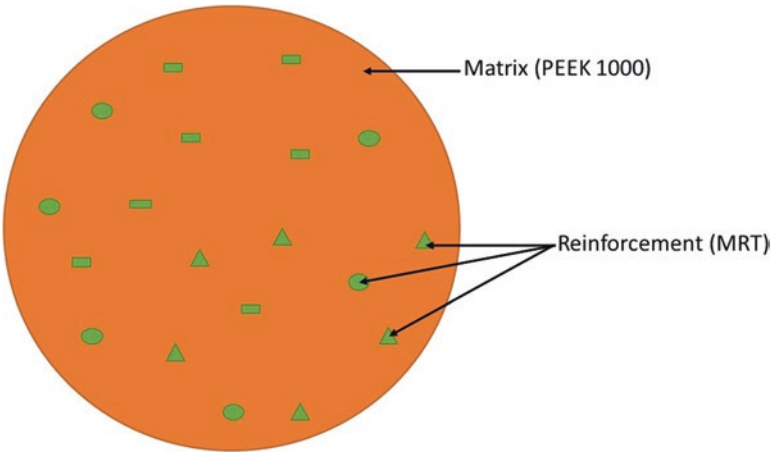

Fig. 10.4 Image of PEEK 1000-composites

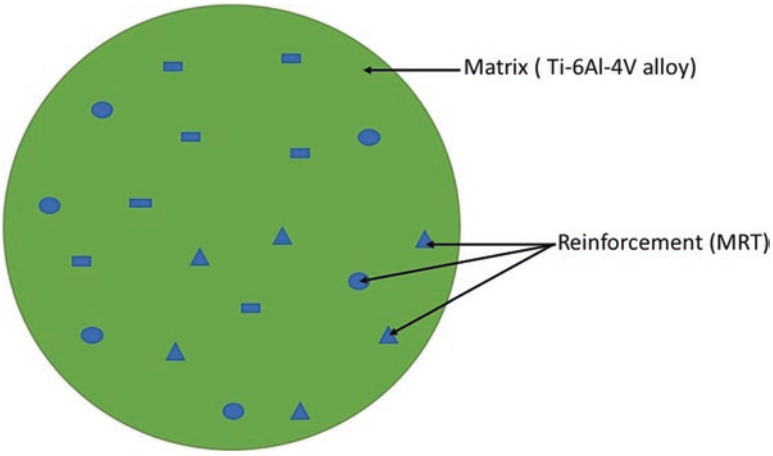

Fig. 10.5 Image of Ti–6Al–4V-composites

Aluminum 6082-T651-CSD and Aluminum 6082-T651-MRT composites, PEEK 1000-CSD and PEEK 1000-MRT composites, and Ti–6Al–4V-CSD and Ti–6Al–4V-MRT composites.

It will be decided what the MMP of the generated composites is, and that information will be utilized to fill out Table 10.4 with data that will be used to simulate models for these various composites.

Table 10.4 The mechanical material properties (MMP) of the aluminum 6082-T651-MRT, PEEK 1000-MRT, and Ti–6Al–4V-MRT composites

MMP	Units	Materials					
		1	2	3	4	5	6
Elastic modulus (E)	GPa	YTBD	YTBD	YTBD	YTBD	YTBD	YTBD
Density (ρ)	kg/m^3	YTBD	YTBD	YTBD	YTBD	YTBD	YTBD
Poisson's ratio (ν)		YTBD	YTBD	YTBD	YTBD	YTBD	YTBD
Coefficient of Kinetic friction (μ)		YTBD	YTBD	YTBD	YTBD	YTBD	YTBD

Key: Aluminum 6082-T651-CSD composite = 1; Aluminum 6082-T651-MRT composite = 2; PEEK 1000-CSD composite = 3; PEEK 1000-MRT composite = 4; Ti–6Al–4V-CSD composite = 5; Ti–6Al–4V-MRT composite = 6; YTBD = Yet to be determined

10.10.2 Methods

10.10.2.1 Scaling and Similitude of Turbine Blade

Utilizing engineering concepts, the simpler turbine blade will be scaled. An SGL-formatted CAD turbine blade model will be created in order to accomplish this. The scaled turbine blade model and the real turbine blade will both have the same geometric similarity, kinematic similarity, and dynamic similarity as a result of the scaling and similitude operations. This is done in an effort to get the printer to manufacture a model of a turbine blade that resembles a real turbine blade. The following phase of the investigation will make use of this scaled model.

10.10.2.2 Optimization in the Abaqus Environment Using TOSCA

It is standard procedure to discover the ideal parameter (in this case, infill density) that satisfies the functional impact tolerance requirements after scaling and simulating the engineering structure (i.e., turbine blade). In this study, sizing optimization tools like SIMULIA Tosca Structure, which integrates optimization technologies in real-world engineering environments as an add-on module easily integrated into the existing Abaqus workflows as shown in Fig. 10.6, will be used instead of trial and error, which is a time-consuming and slow process.

The scaled turbine model from the earlier part will go through an optimization job where the objective function, or infill density, will be chosen and defined for minimization or maximization, and the corresponding restrictions and elements will be defined as design elements. Abaqus will be used for all setups and definitions, with computer-aided engineering (CAE) used for preprocessing (Fig. 10.6).

The model is then automatically updated and adjusted using a robust nonlinear constrained optimizer based on sensitivities obtained using the semi-analytical adjoint method, and the optimization work is then finished by an iterative process. The Abaqus solver will be used to resolve the adjoint equations as well as the finite element equilibrium equations. The final model with optimum infill densities will

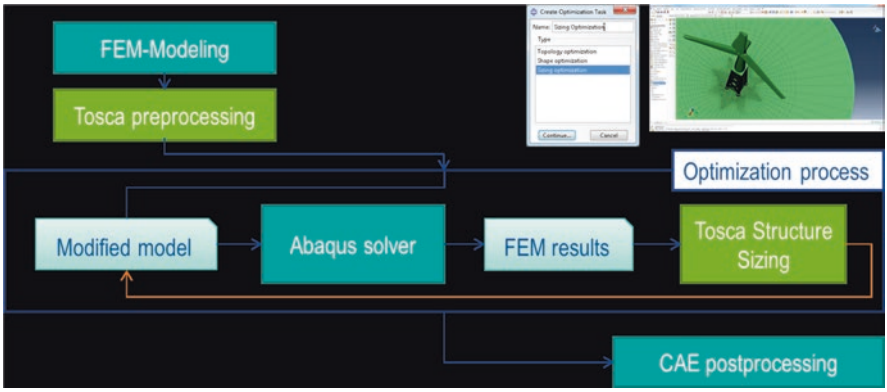

Fig. 10.6 Tosca sizing process workflow [84]

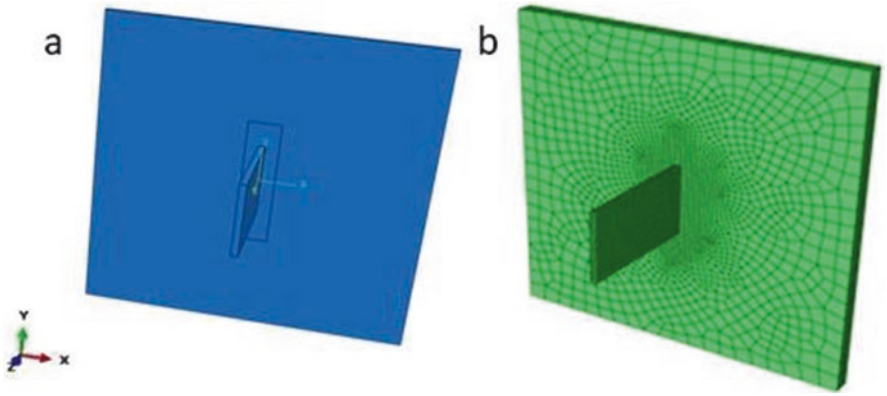

Fig. 10.7 (**a**) The Blade model and interactions, (**b**) Mesh refinement on the whole model: i.e., the turbine blade and the casing

be made available for the CAE postprocessing at the conclusion of the optimization operation.

10.10.2.3 Impact Analysis in Abaqus Based on Tosca's Optimal Solutions

Figure 10.7a depicts a simplified blade model with dimensions of 22 mm in width, 37 mm in length, and 2 mm in thickness. The thickness can range from 2 to 5 mm. In this study, nine different blade materials—aluminum 6082-T651, PEEK 1000, Ti–6Al–4V, aluminum 6082-T651-CSD composite, PEEK 1000-CSD composite, Ti–6Al–4V-CSD composite, aluminum 6082-T651-MRT composite, PEEK 1000-MRT composite, and Ti–6Al–4V-MRT composite—will be impact tested on an aluminum 6082-T651 casing.

Since a clearance distance of 1 mm is permitted between the blade and the casing in the design of an actual aircraft turbine blade, the interactions and predetermined loading will rely on the assembly. As shown in Fig. 10.7a, the analysis of the casing will be fixed for this study, and the blade will be translated to the casing's center with a design clearance of 1 mm.

The actual design of the air engine will have a permissible clearance of 1 mm, whereas the clearance between the blade and casing will be 1 mm. With a time of 0.002 s, the analysis will be done in a dynamically explicit manner. This should provide researchers enough time to monitor the extent of damage the blade causes before it bounces off the casing and causes less damage. Due to the assumption that the blade is a freely detachable blade moving at 255 m/s, there won't be any boundary conditions for it.

It is anticipated that the impact zone of the casing will experience considerable deformation and subsequent elementary distortion as a result of the blade's ballistic impact. So, to obtain a particular mesh and performance, adaptive meshing will be applied (Fig. 10.7b). The stability of the nodes will be examined during a mesh quality check. By making the seeds smaller, a finer mesh will be created to increase the density of the elements. As a result, the partition's mesh size is 1 mm. As illustrated in Fig. 10.8, the mesh refinement will take place at the partitioned section. While the model's nodes and elements will have the following numbers at different

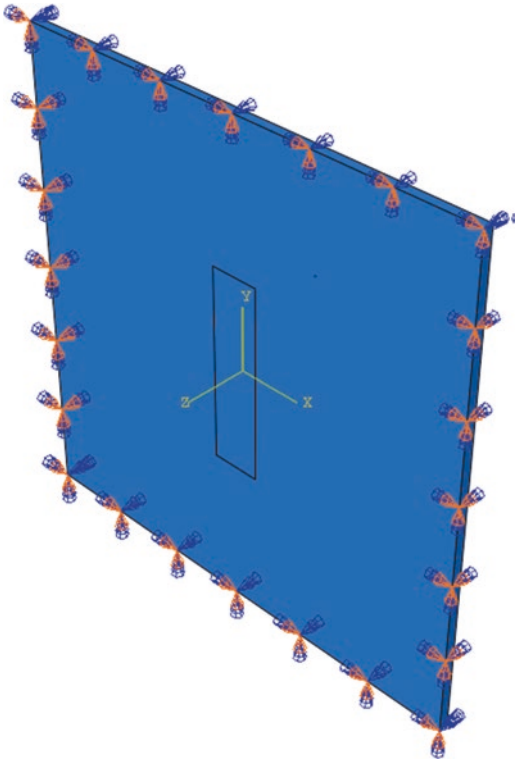

Fig. 10.8 Boundary conditions for Aluminum 6082-T651 alloy casing

case thicknesses (2, 3, 4, and 5): Elements are 5406, 7668, 13,576, and 10,506 respectively, while nodes are 5442, 7612, 10,584, and 13,781 correspondingly.

As demonstrated in Fig. 10.8, the bottom and top of the casing will be prevented from shifting and rotating in the x and y directions while being free to deform. Due to the assumption that the blade is detached from the hub, as was previously mentioned, the blade has free boundary conditions.

10.10.2.4 3D Printing of the Turbine Blade

The simplified turbine blade model that has been optimized and thoroughly examined will be divided into layers that overlap by 35–50 μm to create the turbine blade components. The size of the material's particles will range from 20 to 55 μm. In this study, the turbine blades will be printed using the powder bed additive CSIR Selective Laser Melting (SLM) apparatus for further analysis.

10.10.2.5 Experimental Validation

In order to verify the consistency of the Abaqus results, an experimental impact study will be performed utilizing the Charpy impact tester on the printed optimized/analyzed simplified turbine blade model.

10.10.2.6 Measurements and Microstructural Analysis of Damaged Samples

Scanning Electron Microscopy (SEM)

With the help of scanning electron microscopy (SEM) in the FEI model Inspect F-50 operating in both secondary (SE) and backscattered (BSE) electron modes, it will be possible to determine the spatial distribution of the CSD and MRT in the matrices (Aluminum, PEEK, Ti–6Al–4V alloy), as well as the degree of damage to both unreinforced and reinforced materials. It will be furnished with a Link Analytical ISIS system for elemental analysis, both qualitative and quantitative (EDX). To supplement SEM characterization, a RayScan model 250E computed x-ray microtomography investigation was performed.

Electron Backscatter Diffraction (EBSD)

To evaluate the deformation caused in the unreinforced and reinforced materials in terms of potential phase change, recrystallization, strain hardening, and deformation texture, EBSD will be carried out using a Zeiss model Ultra 55 microscope fitted with an Oxford detector.

X-Ray Diffraction (XRD)

X-ray diffraction (XRD) analysis will be performed in addition using Panalytical's X Pert PRO equipment. Since creating the reinforced composites depends on creating the samples, rigorous procedures will be taken into account at this point.

10.11 Project Plan and Financial Budget

10.11.1 Project Plan

The layout and timeline for the proposed study can be seen in Table 10.5.

10.11.2 Financial Budget

Detailed in Table 10.6 is the estimated budget for the proposed study.

Table 10.5 Layout and timeline for the proposed study

		Year	
S/N	Task name	XXXX	XXXX
1	Registration	WIP	WIP
2	Development of research topic	WIP	WIP
3	Development of research proposal and approval	WIP	WIP
4	Chapter 1	WIP	WIP
6	Chapter 2	WIP	WIP
7	Chapter 3	WIP	WIP
8	Chapter 4	WIP	WIP
9	Chapter 5	WIP	WIP
10	Chapter 6	WIP	WIP
11	Chapter 7	WIP	WIP
12	Chapter 8	WIP	WIP
13	Chapter 9	WIP	WIP
14	Chapter 10	WIP	WIP
15	Colloquium	WIP	WIP
16	Thesis defence	WIP	WIP
17	Production of final dissertation	WIP	WIP
18	Submission	WIP	WIP

Table 10.6 Estimated budget for the proposed study

S/N	General items	Description	Cost (ZAR)
1	Tuition fees	Registration (DEng)	X
		Deng fees	X
2	Study materials	Journals	X
3	Experimentation and model manufacture	Component from Aluminum, PEEK, and Ti–6Al–4V materials and FEA software	X
4	Instrumentation	Data recording instruments, turbine blade parts for impact tolerance measurement	X
	Submission cost	Report binding for at least four copies	X
Grand total			X

References

1. O.A. Akinboade, L.A. Braimoh, International tourism and economic development in South Africa: A Granger causality test. Int. J. Tour. Res. **12**(2), 149–163 (2010)
2. A. Gisario, M. Kazarian, F. Martina, M. Mehrpouya, Metal additive manufacturing in the commercial aviation industry: A review. J. Manuf. Syst. **53**, 124–149 (2019)
3. S. Ford, M. Despeisse, Additive manufacturing and sustainability: An exploratory study of the advantages and challenges. J. Clean. Prod. **137**, 1573–1587 (2016)
4. D.O. Okanigbe, A.P.I. Popoola, T.N. Makua, Determination of physico-chemical and hardness properties of mullite-rich tailings from density separated copper smelter dust for ceramic application, in *TMS 2021 150th Annual Meeting & Exhibition Supplemental Proceedings*, (Springer, Cham, 2021), pp. 1026–1035
5. P.L. Linda, D.O. Okanigbe, A.P.I. Popoola, O.M. Popoola, Characterization of density separated mullite-rich tailings from a secondary copper resource, a potential reinforcement material for development of an enhanced thermally conductive and wear resistant Ti-6Al-4V matrix composite, in *The Proceedings of the 60th International Conference of Metallurgist*. Canada, (2021)
6. M.K. Niaki, F. Nonino, *The Management of Additive Manufacturing*, vol 10 (Springer, 2018), pp. 978–973
7. J.A. Castillo-Robles, A.P. Dimas-Muñoz, J.A. Rodríguez-García, C.A. Calles-Arriaga, E.N. Armendáriz-Mireles, W.J. Pech-Rodríguez, E. Rocha-Rangel, Mechanical and microstructural response of aluminum composites reinforced with ceramic micro-particles. J. Compos. Sci. ***5***(9), 228 (2021)
8. N. Kota, M.S. Charan, T. Laha, S. Roy, Review on development of metal/ceramic interpenetrating phase composites and critical analysis of their properties. Ceram. Int. **48**(2), 1451–1483 (2022)
9. D. Zhao, D. Wu, J. Shi, F. Niu, G. Ma, Microstructure and mechanical properties of melt-grown alumina-mullite/glass composites fabricated by directed laser deposition. J. Adv. Ceram. **11**(1), 75–93 (2022)
10. K.N. Lee, D. Zhu, R.S. Lima, Perspectives on environmental barrier coatings (EBCs) manufactured via air plasma spray (APS) on ceramic matrix composites (CMCs): A tutorial paper. J. Therm. Spray Technol. **30**, 1–19 (2021)
11. S.K. Suleimanov, V.G. Babashov, M.U. Dzhanklich, V.G. Dyskin, M.I. Daskovskii, S.Y. Skripachev, N.A. Kulagina, G.M. Arushanov, Behavior of a heat-protective material based on Al 2 O 3 and SiO 2 fibers under exposure to concentrated solar energy flux. Refract. Ind. Ceram. **61**(6), 675–679 (2021)

12. O. Zaporozhets, V. Isaienko, K. Synylo, PARE preliminary analysis of ACARE FlightPath 2050 environmental impact goals. CEAS Aeronaut. J. **12**(3), 653–667 (2021)
13. N.P. Padture, Advanced structural ceramics in aerospace propulsion. Nat. Mater. **15**(8), 804–809 (2016)
14. J. King, P. Greaves, H. Low, Composite materials in aero gas turbines: Performance potential versus commercial constraint. Aircr. Eng. Aerosp. Technol **70**, 3 (1998)
15. J. Cheung, J. Scanlan, J. Wong, J. Forrester, H. Eres, P. Collopy, P. Hollingsworth, S. Wiseall, S. Briceno, Application of value-driven design to commercial aeroengine systems. J. Aircr. **49**(3), 688–702 (2012)
16. T.D. Ngo, A. Kashani, G. Imbalzano, K.T. Nguyen, D. Hui, Additive manufacturing (3D printing): A review of materials, methods, applications and challenges. Compos. Part B **143**, 172–196 (2018)
17. J. Kraft, S. Kuntzagk, Engine fleet-management: The use of digital twins from a MRO perspective, in *Turbo expo: Power for Land, Sea, and Air*, vol. 50770, (American Society of Mechanical Engineers, 2017), p. V001T01A007
18. G.M. Laskowski, J. Kopriva, V. Michelassi, S. Shankaran, U. Paliath, R. Bhaskaran, Q. Wang, C. Talnikar, Z.J. Wang, F. Jia, Future directions of high fidelity CFD for aerothermal turbomachinery analysis and design, in *46th AIAA Fluid Dynamics Conference*, (AIAA, 2016), p. 3322
19. R. Jansen, C. Bowman, A. Jankovsky, R. Dyson, J. Felder, Overview of NASA electrified aircraft propulsion (EAP) research for large subsonic transports, in *53rd AIAA/SAE/ASEE Joint Propulsion Conference*, (AIAA, 2017), p. 4701
20. S.K. Sinha, S. Dorbala, Dynamic loads in the fan containment structure of a turbofan engine. J. Aerosp. Eng. **22**(3), 260–269 (2009)
21. J. Carter, Simulation software to assess how, why, where and when components will fail, in *2018 Annual Reliability and Maintainability Symposium (RAMS)*, (IEEE, 2018), pp. 1–5
22. B. Strack, V. Nagpal, S. Pai, A software tool subjecting component designs to system-level reliability constraints, in *48th AIAA/ASME/ASCE/AHS/ASC Structures, Structural Dynamics, and Materials Conference*, (AIAA, 2007), p. 2292
23. R. Saltoğlu, *Opportunities of cost reduction and risks of budget overrun in maintenance spending of an airline in the current market conditions*. Doctoral dissertation, Fen Bilimleri Enstitüsü, 2019
24. N. Kedir, C. Gong, L. Sanchez, M.J. Presby, S. Kane, D.C. Faucett, S.R. Choi, Erosion in gas-turbine grade ceramic matrix composites. J. Eng. Gas Turbines Power **141**(1), 011019 (2019). https://doi.org/10.1115/1.4040848
25. A.K. Misra, L.A. Greenbauer-Seng, Aerospace propulsion and power materials and structures research at NASA Glenn Research Center. J. Aerosp. Eng. **26**(2), 459–490 (2013)
26. P.W. Beaumont, On the problems of cracking and the question of structural integrity of engineering composite materials. Appl. Compos. Mater. **21**(1), 5–43 (2014)
27. M. Schwab, H.E. Pettermann, Modelling and simulation of damage and failure in large composite components subjected to impact loads. Compos. Struct. **158**, 208–216 (2016)
28. K. Raju, T.E. Tay, V.B.C. Tan, A review of the FE 2 method for composites. Multiscale Multidiscip. Model. Exp. Des **4**, 1–24 (2021)
29. Y. Sun, Y. Zhang, Y. Zhou, H. Zhang, H. Zeng, K. Yang, Evaluating impact damage of flat composite plate for surrogate bird-strike testing of Aeroengine fan blade. J. Compos. Sci. ***5***(7), 171 (2021)
30. S.W. Ahmed, G. Hussain, K. Altaf, S. Ali, M. Alkahtani, M.H. Abidi, A. Alzabidi, On the effects of process parameters and optimization of interlaminate bond strength in 3D printed ABS/CF-PLA composite. Polymers **12**(9), 2155 (2020)
31. G.D. Goh, Y.L. Yap, H.K.J. Tan, S.L. Sing, G.L. Goh, W.Y. Yeong, Process–structure–properties in polymer additive manufacturing via material extrusion: A review. Crit. Rev. Solid State Mater. Sci. **45**(2), 113–133 (2020)
32. N. Mohan, P. Senthil, S. Vinodh, N. Jayanth, A review on composite materials and process parameters optimisation for the fused deposition modelling process. Virtual Phys. Prototyp. **12**(1), 47–59 (2017)

33. M. Moradi, S. Meiabadi, A. Kaplan, 3D printed parts with honeycomb internal pattern by fused deposition modelling; experimental characterization and production optimization. Met. Mater. Int. **25**(5), 1312–1325 (2019)
34. T. Muthuramalingam, B. Mohan, Application of Taguchi-grey multi responses optimization on process parameters in electro erosion. Measurement **58**, 495–502 (2014)
35. T. Geethapriyan, K. Kalaichelvan, T. Muthuramalingam, Multi performance optimization of electrochemical micro-machining process surface related parameters on machining Inconel 718 using Taguchi-grey relational analysis. La Metallurgia Italiana **4**, 13–19 (2016)
36. İ. Istif, K. Feratoğlu, A. Acar, Investigation of mechanical behaviours of PLA parts manufactured by fused deposition modeling, in *56th ISC of the University of Ruse'17, Ruse, Bulgaristan*, (2017), pp. 26–29
37. N. Singh, I.U.H. Mir, A. Raina, A. Anand, V. Kumar, S.M. Sharma, Synthesis and tribological investigation of Al-SiC based nano hybrid composite. Alex. Eng. J. **57**(3), 1323–1330 (2018)
38. M.I.U. Haq, A. Anand, Dry sliding friction and wear behavior of AA7075-Si 3 N 4 composite. SILICON **10**(5), 1819–1829 (2018)
39. A. Bernard, A. Fischer, New trends in rapid product development. CIRP Ann. **51**(2), 635–652 (2002)
40. M.I.H.C. Abdullah, M.F.B. Abdollah, H. Amiruddin, N. Tamaldin, N.R.M. Nuri, Optimization of tribological performance of hBN/AL2O3Nanoparticles as engine oil additives. Procedia Eng. **68**, 313–319 (2013)
41. C.K. Chua, K.F. Leong, C.S. Lim, *Rapid Prototyping: Principles and Applications (with Companion CD-ROM)* (World Scientific Publishing Company, 2010)
42. M. Vaezi, C.K. Chua, Effects of layer thickness and binder saturation level parameters on 3D printing process. Int. J. Adv. Manuf. Technol. **53**(1), 275–284 (2011)
43. F. Górski, R. Wichniarek, W. Kuczko, P. Zawadzki, P. Buń, Strength of ABS parts produced by fused deposition modelling technology–a critical orientation problem. Adv. Sci. Tecnol. Res. J. **9**(26), 12–19 (2015)
44. L. Li, Q. Sun, C. Bellehumeur, P. Gu, Composite modeling and analysis for fabrication of FDM prototypes with locally controlled properties. J. Manuf. Process. **4**(2), 129–141 (2002)
45. I. Gajdoš, J. Slota, Influence of printing conditions on structure in FDM prototypes. Tehnički Vjesnik **20**(2), 231–236 (2013)
46. A. Bellini, S. Güçeri, Mechanical characterization of parts fabricated using fused deposition modeling. Rapid Prototyp. J. **9**, 252 (2003)
47. S.H. Ahn, C. Baek, S. Lee, I.S. Ahn, Anisotropic tensile failure model of rapid prototyping parts-fused deposition modeling (FDM). Int. J. Mod. Phys. B ***17***(08n09), 1510–1516 (2003)
48. F. Górski, W. Kuczko, R. Wichniarek, Influence of process parameters on dimensional accuracy of parts manufactured using fused deposition modelling technology. Adv. Sci. Tecnol. Res. J. **7**(19), 27–35 (2013)
49. T.F. Abbas, F.M. Othman, H.B. Ali, Influence of layer thickness on impact property of 3D-printed PLA. Int. Res. J. Eng. Technol. (IRJET) **5**, 1–4 (2018)
50. R. Srinivasan, W. Ruban, A. Deepanraj, R. Bhuvanesh, T. Bhuvanesh, Effect on infill density on mechanical properties of PETG part fabricated by fused deposition modelling. Mater. Today: Proc. **27**, 1838–1842 (2020)
51. E. Ebel, T. Sinnemann, Fabrication of FDM 3D objects with ABS and PLA and determination of their mechanical properties. Rapid Technol **2014**(1), 4–22 (2014)
52. M.Q. Tanveer, A. Haleem, M. Suhaib, Effect of variable infill density on mechanical behaviour of 3-D printed PLA specimen: An experimental investigation. SN Appl. Sci. **1**(12), 1–12 (2019)
53. K.N. Gunasekaran, V. Aravinth, C.M. Kumaran, K. Madhankumar, S.P. Kumar, Investigation of mechanical properties of PLA printed materials under varying infill density. Mater. Today: Proc. **45**, 1849–1856 (2021)
54. E. AtiK, C. Meriç, B. Karlik, Determination of yield strength of 2014 Aluminium alloy under aging conditions by means of Artifical neural networks method. Math. Comput. Appl. **1**(2), 16–20 (1996)

55. P.P.N.K.V. Rambabu, N.E. Prasad, V.V. Kutumbarao, R.J.H. Wanhill, Aluminium alloys for aerospace applications, in *Aerospace Materials and Material Technologies*, (Springer, 2017), pp. 29–52
56. P. Mukhopadhyay, Alloy designation, processing, and use of AA6XXX series aluminium alloys. Int. Sch. Res. Not. **2012**, 165082 (2012)
57. C. Kammer, Aluminum and aluminum alloys, in *Springer Handbook of Materials Data*, (Springer, Cham, 2018), pp. 161–197
58. D. Altenpohl, *Aluminum Viewed from Within: An Introduction into the Metallurgy of Aluminum Fabrication* (Aluminium-Verlag GmbH, Konigsallee, 1982), p. 223
59. S.R. Ch, A. Raja, P. Nadig, R. Jayaganthan, N.J. Vasa, Influence of working environment and built orientation on the tensile properties of selective laser melted $AlSi_{10}Mg$ alloy. Mater. Sci. Eng. A **750**, 141–151 (2019)
60. K.G. Prashanth, S. Scudino, J. Eckert, Defining the tensile properties of Al-12Si parts produced by selective laser melting. Acta Mater. **126**, 25–35 (2017)
61. Y. Ou, Q. Zhang, Y. Wei, Y. Hu, S. Sui, J. Chen, X. Wang, W. Li, Evolution of heterogeneous microstructure and its effects on tensile properties of selective laser melted AlSi10Mg alloy. J. Mater. Eng. Perform. **30**(6), 4341–4355 (2021)
62. M.S. Kumar, H.R. Javidrad, R. Shanmugam, M. Ramoni, A.A. Adediran, C.I. Pruncu, Impact of print orientation on morphological and mechanical properties of L-PBF based AlSi7Mg parts for aerospace applications. Silicon **14**, 1–15 (2021)
63. M. Gowda, M. Karthick, S.K. Niketh, M. Kanagil, V. Guptha, A. Bharatish, R. Sharma, Effect of laser parameters on the vibrational characteristics of $AlSi_{10}Mg$ parts produced using selective laser melting (SLM). Lasers Eng. (Old City Publishing) **51**(1–5), p187–203. 17p, (2021)
64. D. Dai, D. Gu, H. Zhang, J. Xiong, C. Ma, C. Hong, R. Poprawe, Influence of scan strategy and molten pool configuration on microstructures and tensile properties of selective laser melting additive manufactured aluminum-based parts. Opt. Laser Technol. **99**, 91–100 (2018)
65. J. Bi, Y.B. Chen, X. Chen, M.D. Starostenkov, G.J. Dong, Densification, microstructural features and tensile properties of selective laser melted AlMgSiScZr alloy from single track to block specimen. J. Cent. South Univ. **28**(4), 1129–1143 (2021)
66. P. Ponnusamy, S.H. Masood, D. Ruan, S. Palanisamy, R.R. Rashid, R. Mukhlis, N.J. Edwards, Dynamic compressive behaviour of selective laser melted $AlSi_{12}$ alloy: Effect of elevated temperature and heat treatment. Addit. Manuf. **36**, 101614 (2020)
67. M. Awd, S. Siddique, F. Walther, Microstructural damage and fracture mechanisms of selective laser melted Al-Si alloys under fatigue loading. Theor. Appl. Fract. Mech. **106**, 102483 (2020)
68. A. Mishra, R. Agarwal, N. Kumar, A. Rana, A.K. Pandey, S.P. Dwivedi, A critical review on the additive manufacturing of aluminium alloys. Mater. Today: Proc. **47**, 4074 (2021)
69. K.C. Bae, K.S. Ha, Y.H. Kim, J.J. Oak, W. Lee, Y.H. Park, Building direction dependence of wear resistance of selective laser melted AISI 316L stainless steel under high-speed tribological environment. Int. J. Adv. Manuf. Technol. **108**, 2385–2396 (2020)
70. P. Wang, S. Yu, J. Shergill, A. Chaubey, J. Eckert, K.G. Prashanth, S. Scudino, Selective laser melting of Al-7Si-0.5 mg-0.5 cu: Effect of heat treatment on microstructure evolution, mechanical properties and Wear resistance. Acta Metall. Sin. (English Letters) **35**, 1–8 (2021)
71. T. Maconachie, M. Leary, P. Tran, J. Harris, Q. Liu, G. Lu, D. Ruan, O. Faruque, M. Brandt, The effect of topology on the quasi-static and dynamic behaviour of SLM $AlSi_{10}Mg$ lattice structures. Int. J. Adv. Manuf. Technol. **118**, 1–20 (2021)
72. A. Patel, V. Venoor, F. Yang, X. Chen, M.J. Sobkowicz, Evaluating poly (ether ether ketone) powder recyclability for selective laser sintering applications. Polym. Degrad. Stab. **185**, 109502 (2021)
73. P. Wang, B. Zou, H. Xiao, S. Ding, C. Huang, Effects of printing parameters of fused deposition modeling on mechanical properties, surface quality, and microstructure of PEEK. J. Mater. Process. Technol. **271**, 62–74 (2019)
74. T. Niino, T. Uehara, Low temperature selective laser melting of high tempertaure plastic powder, in *Proceedings Solid Freeform Fabrication Symposium*, (2015), pp. 866–877

75. Y. Wang, J. Shen, M. Yan, X. Tian, Poly ether ether ketone and its composite powder prepared by thermally induced phase separation for high temperature selective laser sintering. Mater. Des. **201**, 109510 (2021)
76. C.R. Knowles, T.H. Becker, R.B. Tait, Residual stress measurements and structural integrity implications for selective laser melted Ti-6Al-4V: General article. S. Afr. J. Ind. Eng. **23**(3), 119–129 (2012)
77. C. Madikizela, L.A. Cornish, L.H. Chown, H. Möller, Microstructure and mechanical properties of selective laser melted Ti-3Al-8V-6Cr-4Zr-4Mo compared to Ti-6Al-4V. Mater. Sci. Eng. A **747**, 225–231 (2019)
78. J. Yang, H. Yu, Z. Wang, X. Zeng, Effect of crystallographic orientation on mechanical anisotropy of selective laser melted Ti-6Al-4V alloy. Mater. Charact. **127**, 137–145 (2017)
79. D. García-González, M. Rodríguez-Millán, A. Vaz-Romero, A. Arias, High impact velocity on multi-layered composite of polyether ether ketone and aluminium. Compos. Interfaces **22**(8), 705–715 (2015)
80. I.S. Boldyrev, I.A. Shchurov, A.V. Nikonov, Numerical simulation of the aluminum 6061-T6 cutting and the effect of the constitutive material model and failure criteria on cutting forces' prediction. Procedia Eng. **150**, 866–870 (2016)
81. J. Ran, F. Jiang, X. Sun, Z. Chen, C. Tian, H. Zhao, Microstructure and mechanical properties of Ti-6Al-4V fabricated by electron beam melting. Crystals **10**(11), 972 (2020)
82. C. Charles, *Microstructure model for Ti-6Al-4V used in simulation of additive manufacturing*. Doctoral dissertation, Luleå Tekniska Universitet, 2016
83. M. Fellah, M. Labaïz, O. Assala, L. Dekhil, A. Taleb, H. Rezag, A. Iost, Tribological behavior of Ti-6Al-4V and Ti-6Al-7Nb alloys for total hip prosthesis. Adv Tribol. **2014**, 1 (2014)
84. A.A.S. Miguel, P.M. Matos, B.W. Claus, Sizing optimization for industrial applications, in *Proceeding of 11th World Congress on Structural and Multidisciplinary Optimization*, (ACM, 2015), pp. 1–6